

EfficientTDNN: Efficient Architecture Search for Speaker Recognition in the Wild

Rui Wang, Zhihua Wei, Shouling Ji, *Member, IEEE*, Zhen Hong

Abstract—Speaker recognition refers to audio biometrics that utilizes acoustic characteristics for automatic speaker recognition. These systems have emerged as an essential means of verifying identity in various scenarios, such as smart homes, general business interactions, e-commerce applications, and forensics. However, the mismatch between training and real-world data causes a shift of speaker embedding space and severely degrades the recognition performance. Various complicated neural architectures are presented to address speaker recognition in the wild but neglect storage and computation requirements. To address this issue, we propose a neural architecture search-based efficient time-delay neural network (EfficientTDNN) to improve inference efficiency while maintaining recognition accuracy. The proposed EfficientTDNN contains three phases. First, supernet design constructs a dynamic neural architecture that consists of sequential cells and enables network pruning. Second, progressive training optimizes randomly sampled subnets that inherit the weights of the supernet. Third, three search methods, including manual grid search, random search, and model predictive evolutionary search, are introduced to find a trade-off between accuracy and efficiency. Results of experiments on the VoxCeleb dataset show EfficientTDNN provides a vast search space including approximately 10^{13} subnets and achieves 1.55% EER and 0.138 DCF_{0.01} with 565M MACs as well as 0.96% EER and 0.108 DCF_{0.01} with 1.46G MACs. Comprehensive investigation suggests that the trained supernet generalizes cells unseen during training and obtains an acceptable balance between accuracy and efficiency.

Index Terms—Speaker recognition, efficient inference, time-delay neural network, neural architecture search, progressive training, evolutionary algorithm.

I. INTRODUCTION

SPEAKER recognition refers to authenticating the identity of a speaker, given his or her spoken utterances. These systems have emerged as an essential means of verifying identity in various scenarios, such as smart homes, general business interactions, e-commerce applications, and forensics. However, since speech varies from person to person and transmits in different situations, a crucial issue is a substantial mismatch between the training and real-world data [1]. In the wild, speech quality is severely degraded, and speech variability is drastically changed [2]. In such a condition, speech recordings can be of arbitrary forms caused by different variability sources, such as voice channels, environmental

noises, speaking styles, and physiological states of speakers. It gives rise to a challenge of speaker recognition in the wild.

One solution to speaker recognition in the wild is to improve the effectiveness of the speaker embeddings. Existing studies have shown that enhancing network architecture design helps boost speaker recognition performance. For example, very deep convolutional networks (VGG)-style architectures are proposed to learn speaker-discriminative embeddings [3], [4]. Deep residual neural (ResNet) architectures improve speaker embeddings by introducing shortcut connections [5], [6]. Time-delay neural network (TDNN) utilizes multisplICE temporal contexts to extract discriminative speaker vectors [7], [8], [9]. Dense connection is introduced to strengthen feature propagation to help the network integrate multiple branches with short-term and long-term contexts [10], [11]. However, those either modified from other tasks or have inferior runtime with explosive memory requirement may not be optimal for speaker recognition. A direct consequence is a challenging problem of efficient inference across various constraints.

Since devices require diverse constraints, manual design is not practical and often insufficient to explore immense possibilities. To enable efficient processing to meet different efficiency constraints while maintaining accuracy, neural architecture search (NAS) appears as a practical tool that enables researchers and engineers to design effective architectures and find their associated weights for efficient inference in an automatic manner [12]. This goal has led to notable improvements in CNNs architectures on standard image classification benchmarks [13]. However, since the design of search spaces is crucial and needs to adjust for different tasks [14], directly borrowing the neural cell candidates from the computer vision community may lead to the complex search method and inferior accuracy. Accordingly, it is still challenging to bridge NAS and speaker recognition.

This paper proposes a neural architecture search-based efficient time-delay neural network (EfficientTDNN) to achieve efficient inference for speaker recognition in the wild. As shown in Figure 1, there are three phases: designing a proper search space, devising an effective training method, and developing an efficient search algorithm. First, we borrow the design of TDNN to construct a search space since the TDNN architecture is an active area of speaker recognition and has consistently achieved state-of-the-art performance. Second, the built supernet is trained in a once-for-all manner via multi-condition data augmentation, from which specialized subnets are sampled without additional training. Third, several search algorithms are introduced equipped with an accuracy predictor and efficiency estimator, which help accelerate search to meet

Rui Wang, Zhihua Wei are with the Department of Computer Science and Technology, Tongji University, Shanghai 201804, China (e-mail: rwang@tongji.edu.cn; zhihua_wei@tongji.edu.cn)

Shouling Ji is with the Institute of Cyber Security Research, College of Computer Science & Technology, Zhejiang University, Hangzhou 310027, China (e-mail: sji@zju.edu.cn)

Zhen Hong is with the Institute of Cyberspace Security, and the College of Information Engineering, Zhejiang University of Technology, Hangzhou 310023, China. (e-mail: zhong1983@zjut.edu.cn)

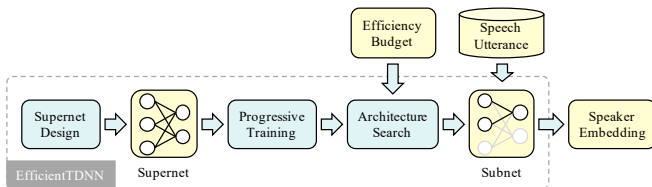


Fig. 1. A flowchart of EfficientTDNN.

different requirements for devices. Experiments are conducted on the popular VoxCeleb datasets to demonstrate the effectiveness of EfficientTDNN.

The contributions of this paper are summarized as follows.

- EfficientTDNN is proposed as a NAS-powered alternative to automatically design efficient architectures for speaker recognition in the wild. EfficientTDNN is powered by an accuracy predictor and efficiency estimator.
- A novel supernet containing dilated convolution, residual connection, dense connection, and Res2Net block is established and supports multiple dynamic dimensions, including depth, width, and kernel size.
- On top of the discovery that the supernet generalizes unseen sizes of micro architectures, several search algorithms with different-grained spaces are introduced to demonstrate that the trained supernet can achieve an acceptable trade-off between accuracy and efficiency.

The rest of this paper is organized as follows. In Section II, we discuss the related work regarding the existing approaches to design efficient neural networks. The notations and the problem formulation are given in Section III. We present the proposed EfficientTDNN in Section IV. Subsequently, the performance of the proposed method is evaluated on a large-scale speaker dataset in Section V. Sensitivity analysis of architecture search is conducted to investigate multiple factors in VI. Finally, we conclude this paper in Section VII.

II. RELATED WORK

A. Speaker Neural Architectures

The rapid development of deep neural networks (DNN) has claimed its domination in the area of speaker recognition. In particular, for speaker recognition in the wild, deep neural networks have successfully achieved state-of-the-art performance on challenging benchmarks, including SITW [2], SRE 2018 [15], and VoxCeleb [16], [17], [18]. For example, McLaren et al. [19] use DNN to extract bottleneck features to enhance robustness to microphone speech. Huang et al. [20] apply a VGG-style CNN to learn an embedding via triplet loss. Ramoji et al. [21] extract neural embeddings from TDNN trained on a speaker discrimination task. Xie et al. [22] use thin-ResNet with GhostVLAD layer to investigate the effect of utterance length on the ‘in the wild’ data. Garcia-Romero et al. [5] propose a wider ResNet by increasing channels in the early stages and achieve state-of-the-art performance. Desplanques et al. [23] utilize several enhancements to TDNN, including residual connection, dense connection, and channel-dependent frame attention, which aggregate and propagate features of different hierarchical levels.

TABLE I
FREQUENTLY USED NOTATIONS

Notation	Description
\mathcal{S}	search space
\mathcal{A}	supernet constructed from \mathcal{S}
a	a subnet sampled from the supernet, $a \in \mathcal{A}$
\mathbb{S}	subnet sampler used to sample a subnet, $a \leftarrow \mathbb{S}(\mathcal{A})$
$W_{\mathcal{A}}$	weights of the supernet
w_a	weights of a network or subnet
\mathcal{L}	loss function
\mathcal{D}	dataset
D	depth of a network or a sequence of layers
K	kernel size of a convolution layer
C	width of a convolution or linear layer
v_i	a cell in an architecture
$v_{i \rightarrow j}$	a sequence of cells $v_i, v_{i+1}, \dots, v_j, j > i$

B. Neural Architecture Search

NAS technique provides a systematic methodology that designs neural architecture automatically. In prior works, Zoph et al. [12] propose an RL-based approach to find an architecture that achieves state-of-the-art performance. However, it is computationally expensive, requiring thousands of different architectures to be trained from scratch. To avoid prohibitive computation, Bender et al. [24] propose a simple weight sharing for one-shot architecture search. Liu et al. [13] formulate the problem of architecture search in a differentiable manner, which is orders of magnitude faster than non-differentiable techniques. Since these architectures optimized on proxy tasks are not guaranteed to be optimal on the target task, Cai et al. [25] propose to directly learn the architectures without any proxy while handling hardware objectives via regularization loss. Subsequently, once-for-all [26] is proposed to further reduce the computational cost by decoupling training and search while enabling diverse architectural settings without additional training. In speaker recognition, AutoSpeech [27] and Auto-Vector [28] construct search spaces containing 2D operations from the computer vision community apply differentiable architecture search to the supernet.

III. PROBLEM FORMULATION

A. Basic Notations

We give the basic notations and their meanings in Table I, where \mathcal{S} , \mathcal{A} , a , and \mathbb{S} relate to architectures, $W_{\mathcal{A}}$ and w_a are weights of architectures, \mathcal{L} and \mathcal{D} are used for training algorithm, D , K , and C are variable dimensions, v_i and $v_{i \rightarrow j}$ represent cells sampled from the supernet.

B. Speaker Recognition in the Wild

All audio excerpts for speaker recognition in the wild represent the original ‘wild’ audio conditions, such as real noise, reverb, vocal effort, compression artifacts, and unconstrained duration. Popular databases are SITW [2], VoxCeleb1 [16], and VoxCeleb2 [17], which are collected from open-source media. For DNN-based systems, there are several solutions. These can be classified into two aspects, namely, architecture design [5], [23] and training algorithm [29]. The former

highlights various design of pooling operations and cross-layer connection, while the latter emphasizes diverse loss functions [30] and data augmentation [31], [32], [33].

C. Neural Architecture Search

Neural architecture search aims to solve two subproblems to find a trained architecture with optimal performance. The first subproblem is weights optimization on the training set, and the second one is architecture search on the validation set. The weight sharing technique provides computationally affordable solutions to NAS. It involves training a supernet that contains all searchable architectures as its subnets, and all subnets inherit weights directly from the supernet. Weight sharing approaches are broadly classified into two categories depending on whether the supernet training and architecture search are coupled or decoupled into two sequential stages. The coupled method suffers from a weak ranking correlation [34]. It is probably a consequence of the optimization gap between the supernet and its subnets [14]. However, the decoupled one uses subnets performance to select architectures during search and makes real-world requirements feasible, such as parameters, multiply-accumulate operations (MACs), and latency.

In summary, the efficient architecture search problem for speaker recognition in the wild can be formulated as a two-stage optimization problem.

- 1) Supernet weights optimization

$$W_{\mathcal{A}} = \arg \min_{W_{\mathcal{A}}} \mathcal{L}_{\text{train}}(\mathcal{A}, W_{\mathcal{A}}) \quad (1)$$

- 2) Subnets search

$$a^* = \arg \min_{a \in \mathcal{A}} \text{Metric}_{\text{val}}(a; W_{\mathcal{A}}(a)) \quad (2)$$

where $\text{Metric}_{\text{val}}(\cdot)$ can be diverse, such as error, parameters, MACs, and latency.

IV. EFFICIENT ARCHITECTURE SEARCH METHOD

In this paper, an efficient architecture search method, namely, EfficientTDNN, is proposed to address the NAS challenge of speaker recognition in the wild. It consists of three phases: search space design, weights optimization, and architecture search. EfficientTDNN starts with a supernet created by multiple enhancements to TDNN architectures. The dynamic properties of architectures enable subnets sampling concerning depth, kernel, and width. Subsequently, a progressive training method integrated with multi-condition data augmentation is proposed to help the supernet adapt ‘wild’ speech and obtain efficient subnets. Finally, with different search space grains, several search algorithms are introduced to demonstrate the effectiveness of the trained supernet and achieve a trade-off between accuracy and efficiency.

A. Search Space

There are two steps to design a search space as an extractor of speaker embeddings: the macro and micro architectures of the space. The macro architecture is a supernet that determines

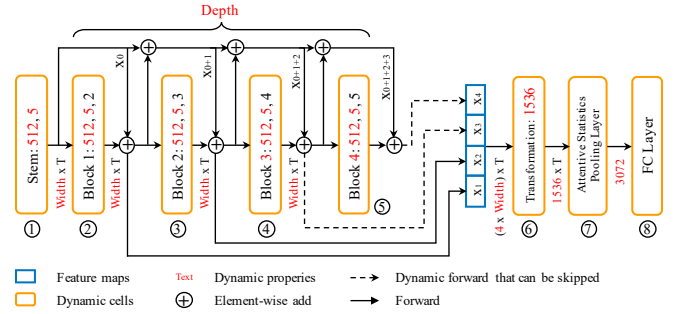


Fig. 2. An overview of the supernet of EfficientTDNN.

the overall backbone of the extractor, while the micro architectures are cells that determine the details of each network unit.

Definition 1 (Supernet). *Supernet is an over-parameterized neural network that contains dynamic components and enables sampling subnets with different architectures.*

The supernet of EfficientTDNN is derived from the design of ECAPA-TDNN [23] that contains residual connections [35], dense connections [10], squeeze-and-excitation (SE) blocks [36], and Res2Net blocks [37]. As illustrated in Figure 2, the supernet is shallow with eight cells, while it is wide with 512 channels in $v_{1 \rightarrow 5}$ and 1,536 features in $v_{6 \rightarrow 8}$.

- 1) v_1 : a stem of input supports dynamic kernel and width.
- 2) $v_{2 \rightarrow 5}$: a stack of blocks that contain Res2Net and SE supports dynamic depth, kernel, and width.
- 3) v_6 : a transformation of concatenated features supports dynamic width.
- 4) v_7 : attentive statistics pooling layer has dynamic width determined by v_6 output.
- 5) v_8 : a fully connected layer (FC) of extracting an embedding has dynamic width determined by v_7 output.

It represents that cells with the dynamic depth are $v_{2 \rightarrow 5}$, cells with the dynamic kernel are $v_{1 \rightarrow 5}$, and cells with the dynamic width are $v_{1 \rightarrow 6}$. On the other hand, v_7 and v_8 are determined by v_6 width, which means they are constrained.

Compared to the original ECAPA-TDNN [23], there are mainly two differences. First, two blocks of v_4 and v_5 can be skipped. Second, kernels of $v_{1 \rightarrow 5}$ are expanded to 5.

The supernet supports dynamic depth, kernel, and width. Specifically, the depth is the number of blocks, where $D \in \{2, 3, 4\}$. It reduces as the last d blocks are skipped, where $d \in \{0, 1, 2\}$. The kernel is the kernel size of the convolution layers in the stem and the middle layer at each block, $K \in \{1, 3, 5\}$. The width is the number of channels or features in $v_{1 \rightarrow 8}$, where $C \in \{C_{\min}, C_{\min} + c, \dots, C_{\max} - c, C_{\max}\}$, C_{\min} is the given minimum width, C_{\max} is the maximum width, and c is an increasing step. We give that $C_{\min} = 128$ and $C_{\max} = 512$ for $v_{1 \rightarrow 5}$ as well as $C_{\min} = 384$ and $C_{\max} = 1536$ for $v_{6 \rightarrow 8}$.

Definition 2 (Degrees of freedom). *Degrees of freedom are the number of independent dimensions that are allowed variable in the formal description of the architecture of the supernet.*

According to Definition 2, the designed supernet has $1 + 5 + 6 = 12$ degrees of freedom, i.e., the depth has 1 degree, the kernel has 5 degrees, and the width 6 degrees.

Definition 3 (Subnet). *Subnet is a neural network that is sampled from the supernet and can be encoded as a 3-tuple of elements of degrees of freedom of the network, $a \equiv (D, \mathbf{K}, \mathbf{C}) \in \mathcal{A}$, where $\mathbf{K} = \{K_i\}_{i=1}^{D+1}$, $\mathbf{C} = \{C_i\}_{i=1}^{D+2}$, and the subscript i of K and C is the number of cells.*

For example, $(3, \{3\}_{i=1}^4, \{256\}_{i=1}^4 \cup \{768\})$ represents a subnet of 3 blocks with kernel sizes of 3, where v_5 is skipped. The width of stem and blocks are 256, while others are 768. Furthermore, the bound of the sampled architectures can be summarized: the largest subnet sampled from the supernet is $(4, \{5\}_{i=1}^5, \{512\}_{i=1}^5 \cup \{1536\})$, while the smallest subnet is $(2, \{1\}_{i=1}^3, \{128\}_{i=1}^3 \cup \{384\})$.

We consider the number of subnets as the size of space.

Definition 4 (Sizes of space). *Sizes of space are the number of independent subnets that are derived from a supernet.*

For example, the variable depth, kernel, and width lead to $145 \times ((3 \times 49)^3 + (3 \times 49)^4 + (3 \times 49)^5) \approx 1.0 \times 10^{13}$ subnets in a space of $c = 8$ while $10 \times ((3 \times 4)^3 + (3 \times 4)^4 + (3 \times 4)^5) \approx 2.7 \times 10^6$ subnets in a space of $c = 128$.

Figure 3 illustrates the details of dynamic cells. It is clear to demonstrate how a subnet or a forward path is generated from the supernet. There are five different types of cells: *stem*, *block*, *transformation*, *pooling*, and *FC*.

- 1) *Stem* is a Conv1d followed by ReLU and batchnorm1d (BN1d), as Conv1dReLUBN. The size of the input is fixed with C_0 channels and T frames, i.e., $C_0 \times T$. The input is first expanded to C_1 channels. Channel-wise operations of ReLU and BN1d are then performed. The output is generated with the size of $C_1 \times T$, where $C_1 \in [128, 512]$. The kernel size is dynamic and is chosen from $\{1, 3, 5\}$.
- 2) *Block* consists of three parts, where the first and last parts are Conv1dReLUBN with the kernel sizes of 1, and the middle part is a dilated convolution layer with a Res2Net module followed by ReLU and BN1d. The first part expands the input of $C_1 \times T$ to $C_2 \times T$, where $C_2 \in [128, 512]$. Also, there can be four different C_2 as four blocks in the supernet. The output from Res2Net has the same size as the input, and then it is reduced to $C_1 \times T$ by the last part. Thus, the sizes of input and output are equal. The dynamic kernel of the Res2Net is done as similar as that of *Stem*.
- 3) *Transformation* is a Conv1d followed by ReLU. The splices of the output of those available cells within $v_{2 \rightarrow 5}$ are concatenated and serve as the input of this cell. The input is first expanded to $C_3 \times T$ and then is performed using ReLU, where $C_3 \in [384, 1536]$.
- 4) *Pooling* contains an attention module and a temporal statistics operation followed by BN1d. The attention module calculates the importance of features in a channel-wise manner across time via a bottleneck in the form of Conv1d with the kernel size of 1. Given the importance of each frame, the weighted statistics

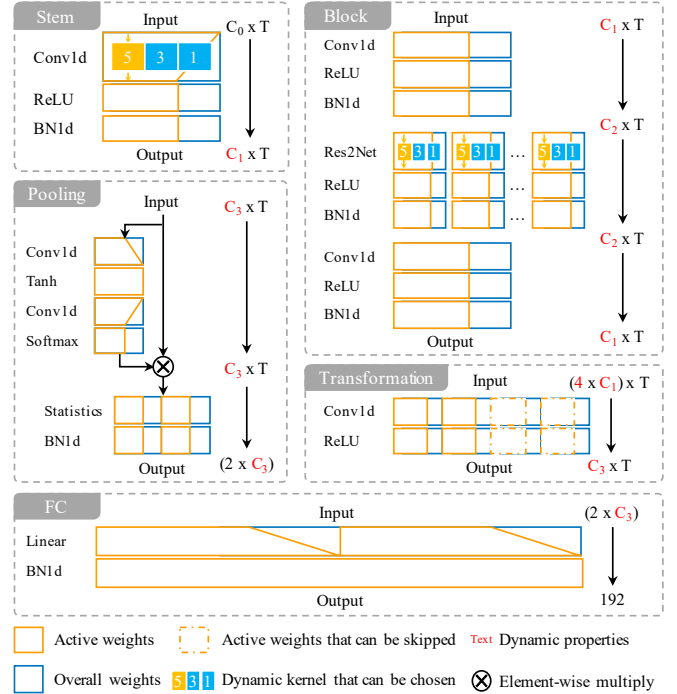


Fig. 3. The details of micro architectures including stem, blocks, transformation, pooling, and FC. The orange and blue boxes are active and overall weights, respectively. The red text points to the variable input and output size at a cell and bridges the forward path.

of each channel that is a concatenated vector of mean and standard deviation are calculated, which convert the input from $C_3 \times T$ to $2C_3$.

- 5) *FC* consists of a linear layer and a BN1d, which extracts an embedding that represents the identity of a speaker.

These dynamic components can be decomposed into three basic operations: dynamic Conv1d, BN1d, and linear layer. These dynamic operations are the same as the traditional ones but perform with active weights. The weights of dynamic Conv1d at the i -th input channel and the j -th output channel are derived from the overall weights W as described one of follows.

$$\begin{aligned} \text{weight}(j, i) &= W[:, C_{\text{out}}, : C_{\text{in}}] \\ \text{weight}(j, i) &= W[\text{out}, \text{in}] \end{aligned}$$

where **out** and **in** are active indexes, respectively.

Likewise, the dynamic BN1d calculates mini-batch mean and variance with active channels. The dynamic linear layer ignores inactive weights associated with dropped inputs.

However, sampling a subnet from the supernet is challenging since the weights of dynamic components are shared and require to adapt to each other. For example, the weights of the centering sub kernel serve the subnets with different distribution identical degrades the performance of subnets with different depth, kernel, or width.

Inspired by [26], a dynamic kernel of Conv1d is introduced to address this challenge. As shown in Figure 4, a linear transformation is applied to the center of a larger kernel, and then a

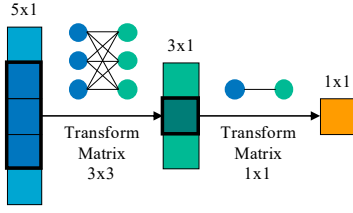


Fig. 4. Kernel transformation matrices for dynamic kernels.

weighted smaller kernel is created. For example, the center of a kernel 5 serves a kernel 3. Kernel transformation matrices are presented as (3) and (4). Separate kernel transformation matrices are used for different sizes, e.g., $W_K^1 \in \mathbb{R}^{3 \times 3}$ is applied to kernel 5, while $W_K^2 \in \mathbb{R}^{1 \times 1}$ is applied to kernel 3. There are extra parameters in the supernet among $v_{1 \rightarrow 5}$, which is negligible compared to the whole architecture. Also, these parameters are eliminated when a subnet is derived from the supernet by performing kernel transformations.

$$W_{\text{kernel}}^1 = W_K^1 \text{Center}(W_{\text{kernel}}) \quad (3)$$

$$W_{\text{kernel}}^2 = W_K^2 \text{Center}(W_{\text{kernel}}^1) \quad (4)$$

where $W_{\text{kernel}} \in \mathbb{R}^{5 \times 1}$, $W_K^1 \in \mathbb{R}^{3 \times 1}$, and $W_K^2 \in \mathbb{R}^{1 \times 1}$ denote the weights of the kernel sizes of $\{1, 3, 5\}$, respectively. W_K^1 and W_K^2 are initialized in the form of an identity matrix.

Regardless of the number of nonzero weights and nonzero MACs that reflect the theoretical minimum requirements of storage and computation [38], the inference time complexity of a subnet $O(a)$ can be summarized as Theorem 1. Therefore, the minimum and maximum efficiency can be estimated directly by performing inference on the smallest and largest architectures.

Theorem 1 (Bound of inference time). *Let $a \in \mathcal{A}$, then the inference time of a subnet with the minimum depth, the minimum kernel size, and the minimum width is a lower bound of $O(a)$, while the inference time of a subnet with the maximum depth, the maximum kernel size, and the maximum width is an upper bound of $O(a)$ so that $\forall a \in \mathcal{A}$ we have*

$$O(a_{\min}) \leq O(a) \leq O(a_{\max})$$

where

$$a_{\min} \equiv (D_{\min}, \mathbf{K}_{\min}, \mathbf{C}_{\min})$$

$$a_{\max} \equiv (D_{\max}, \mathbf{K}_{\max}, \mathbf{C}_{\max})$$

Proof: By Definition 3, the minimum and maximum subnets are $(D_{\min}, \mathbf{K}_{\min}, \mathbf{C}_{\min})$ and $(D_{\max}, \mathbf{K}_{\max}, \mathbf{C}_{\max})$, respectively, a_{\min} and a_{\max} for clarity.

$$a_{\min} = (2, \{1, 1, 1\}, \{128, 128, 128, 384\})$$

$$a_{\max} = (4, \{5, 5, 5, 5, 5\}, \{512, 512, 512, 512, 512, 1536\})$$

It clearly indicates that $\exists a_1, a_2 \in \mathcal{A}$ we have

$$O(a_1) = O(a_{\min})$$

$$O(a_2) = O(a_{\max})$$

Let $a \in \mathcal{A}$, the inference time of a comes from static units and dynamic components as Definition 1 and 3. The inference

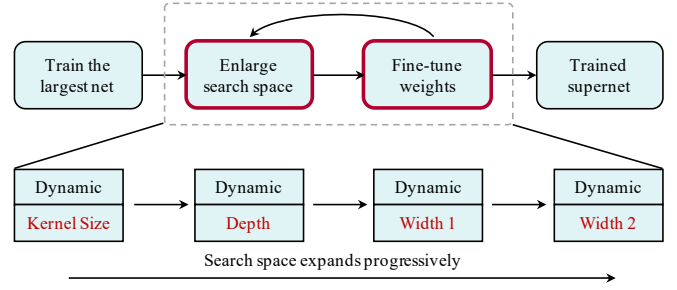


Fig. 5. An overview of the progressive training process. The maximal network is first trained as the initial weights for fine-tuning. Then, the search space expands in a sequence of kernel, depth, and width, where width 1 ranges the width low to half, while width 2 ranges low to a quarter.

time of those static units is constant, but the inference time of the dynamic components is affected by dynamic transformations.

As the transformations of (3) and (4), $\forall a \in \mathcal{A}$, for $v_{1 \rightarrow 5}$ we have

$$W_{\text{kernel}}(a) \in \{W_{\text{kernel}}^2, W_{\text{kernel}}^1, W_{\text{kernel}}\}$$

By the formulation of the dynamic Conv1d, the inference time increases as the kernel size enlarges and the channel expands. This implies that for $v_{1 \rightarrow 5}$ we have

$$O(W_{\text{kernel}}^2) < O(W_{\text{kernel}}^1) < O(W_{\text{kernel}})$$

The dynamic components of a_{\max} and a_{\min} involve W_{kernel} and W_{kernel}^2 , respectively, for $v_{1 \rightarrow 5}$.

Furthermore, the inference time of dynamic BN1d and linear layer increase as the size of input and output enlarge. Thus $\forall a \in \mathcal{A}$ we conclude

$$O(a_{\min}) \leq O(a) \leq O(a_{\max})$$

□

B. Weights Optimization

The supernet comprises various subnets of different sizes where small subnets are nested in large subnets. The weights optimization problem (1) is decomposed into five stages as formulated in (5) to mitigate interference between the subnets and overcome the challenge of optimizing a huge search space. A progressive training method via single path one-shot routing [39] is proposed to solve these subproblems separately.

$$W_{\mathcal{A}^-} = \arg \min_{W_{\mathcal{A}^-}} \mathcal{L}_{\text{train}}(\mathcal{A}^-, W^-) \quad (5)$$

where \mathcal{A}^- is a variant of the search space with the specific sampling dimensions, and W^- represents its weights. For example, $\mathcal{A}^{\text{kernel}}$ is a supernet with variable kernel sizes, and W^{kernel} is its weights.

As shown in Figure 5, the proposed training method enforces a training order from large subnets to small subnets in a progressive manner to overcome the limitation, i.e., dramatically enlarging search space makes the weights of cells hard to adapt to each other. First, the largest network is optimized with the maximum kernel size (i.e., 5), depth (i.e., 4), and

Algorithm 1: Progressive Training Method

Input: supernet \mathcal{A} , weights $W_{\mathcal{A}}$, subnet sampler \mathbb{S} , loss function \mathcal{L} , training data $\mathcal{D}_{\text{train}}$

Output: the trained weights of the supernet $W_{\mathcal{A}}$

- 1 Set sampling space $s \leftarrow \emptyset$ for \mathcal{A}
- 2 Initialize the weights of the supernet $W_{\mathcal{A}}$
- 3 **for** task in $\{\textit{largest}, \textit{kernel}, \textit{depth}, \textit{width}\}$ **do**
- 4 **if** task is *largest* **then**
- 5 $\mathcal{A} \leftarrow$ set \mathcal{A} as the largest architecture
- 6 **else if** task is *kernel* **then**
- 7 $s \leftarrow s \cup \{\textit{kernel} : \{1, 3, 5\}\}$
- 8 **else if** task is *depth* **then**
- 9 $s \leftarrow s \cup \{\textit{depth} : \{2, 3, 4\}\}$
- 10 **else**
- 11 **for** phase in $\{1, 2\}$ **do**
- 12 **if** phase is 1 **then**
- 13 $s \leftarrow s \cup \{\textit{width} : \{0.5, 0.75, 1\}\}$
- 14 **else**
- 15 $s \leftarrow s \cup \{\textit{width} : \{0.25, 0.35\}\}$
- 16 **end**
- 17 **end**
- 18 **end**
- 19 $W_{\mathcal{A}} \leftarrow$ update $W_{\mathcal{A}}$ using Algorithm 2
- 20 **end**
- 21 **return** $W_{\mathcal{A}}$

TABLE II
SIZES OF SPACE IN TRAINING TASKS

Stage	Dynamic Dimension	Sizes of Space
<i>largest</i>	\emptyset	1
<i>kernel</i>	$\cup \{\textit{kernel} : \{1, 3, 5\}\}$	243
<i>depth</i>	$\cup \{\textit{depth} : \{2, 3, 4\}\}$	351
<i>width 1</i>	$\cup \{\textit{width} : \{0.5, 0.75, 1\}\}$	199,017
<i>width 2</i>	$\cup \{\textit{width} : \{0.25, 0.35\}\}$	4,066,875

width (i.e., 512). Next, the supernet is fine-tuned progressively to support smaller subnets by gradually expanding the search space. Specifically, after the largest architecture is trained, the dynamic kernel is supported and is chosen from $\{1, 3, 5\}$ at $v_{1 \rightarrow 5}$, while the depth and width keep the maximum value. Subsequently, the dynamic depth and width are supported. On the other hand, since the range of dynamic width is large, the search space of width is separate by taking half of the maximum value as the dividing line. According to Definition 4, sizes of space at different stages are listed in Table II, which reveals a significant increase in sizes of space after *depth*.

The proposed training approach divides the search space into five sequential parts and separately trains those weights as shown in Algorithm 1, including *largest*, *kernel*, *depth*, *width 1*, and *width 2* in sequence. During each subprocess, the subnets sampler \mathbb{S} samples one or more forward paths randomly as the uniform sampling of a single path in [39], which is employed to update a part of weights in the supernet.

Specifically, in the task of *largest*, the supernet retains the maximum architecture, where the weights but W_K^1 and W_K^2 are updated. Next, in *kernel*, the forward path allows sampling subnets from multiple kernel sizes, e.g., $\{1, 3, 5\}$. As outlined in Algorithm 2, the weights of a sampled forward path are updated at every training step, including W_K^1 and W_K^2 for

Algorithm 2: Dynamic Path Training

Input: weights $W_{\mathcal{A}}$, subnet sampler \mathbb{S} , sampling space s , forward paths M , loss function \mathcal{L} , training data $\mathcal{D}_{\text{train}}$, epochs T , data augmentation \mathcal{F}_{aug}

Output: the trained weights $W_{\mathcal{A}}$

- 1 **def** DynamicTrain($W_{\mathcal{A}}, \mathbb{S}, s, M, \mathcal{L}, \mathcal{D}_{\text{train}}, T, \mathcal{F}_{\text{aug}}$):
- 2 $\mathbb{S} \leftarrow$ update \mathbb{S} by using s
- 3 $t \leftarrow 0$
- 4 **while** $t < T$ **do**
- 5 **for** batch _{i} in $\mathcal{D}_{\text{train}}$ **do**
- 6 $f_{\text{aug}} \leftarrow$ choose from \mathcal{F}_{aug} randomly
- 7 batch _{i} $\leftarrow f_{\text{aug}}$ (batch _{i})
- 8 $\nabla = \emptyset$
- 9 **for** $i = 1$ to M **do**
- 10 $a \leftarrow \mathbb{S}(\mathcal{A})$
- 11 $w \leftarrow W_{\mathcal{A}}(a)$
- 12 $\mathcal{L} \leftarrow$ cross-entropy on batch _{i}
- 13 $\nabla \leftarrow \nabla \cup \partial \mathcal{L} / \partial w$
- 14 **end**
- 15 $W_{\mathcal{A}} \leftarrow$ update $W_{\mathcal{A}}$ using Adam with ∇
- 16 **end**
- 17 $t \leftarrow t + 1$
- 18 **end**
- 19 **return** $W_{\mathcal{A}}$
- 20 **end**

$v_{1 \rightarrow 5}$. Forward paths of M are applied to aggregate gradients, and weights are updated along these forward paths. The task of *depth* is performed after the task of *kernel*. It makes the number of blocks variable between 2 and 4. The task of *width* expands carefully and is divided into two stages. The width of $\{0.5, 0.75, 1.0\}$ and $\{0.25, 0.35\}$ of the maximum value are sequentially added into sampling space.

C. Architecture Search

After the supernet is trained, the next stage is to derive the specialized subnet for the given constraints. Based on (2), architecture search aims to find the optimal architecture that optimizes the accuracy while satisfies the efficiency constraints (6). This stage, similar to [26], does not require retraining since EfficientTDNN decouples weights optimization from architecture search. It significantly reduces the computational burden and makes various search algorithms feasible.

$$\begin{aligned} & \arg \max_{a \in \mathcal{A}} \text{ACC}_{\text{val}}(a; W_{\mathcal{A}}(a)) \\ & \text{s.t. Efficiency}(a) \leq \text{Budget} \end{aligned} \quad (6)$$

where ACC_{val} is an accuracy metric, Efficiency is an efficiency metric, and Budget is its budget. As shown in Figure 6, these indices are calculated based on a subnet encoded as Definition 3, which is used to measure accuracy via architecture decoding, predict accuracy via one-hot encoding, and estimate efficiency via layer-wise encoding.

The design of sampling space and search strategy play essential roles in solving search problems. The former determines the solution space to be searched, and the latter determines the method to be adopted. Three modes of the search space are considered to investigate the impact of sampling space: the grid, coarse-grained, and fine-grained spaces. In the grid space, depth, kernel, and width are supposed as three

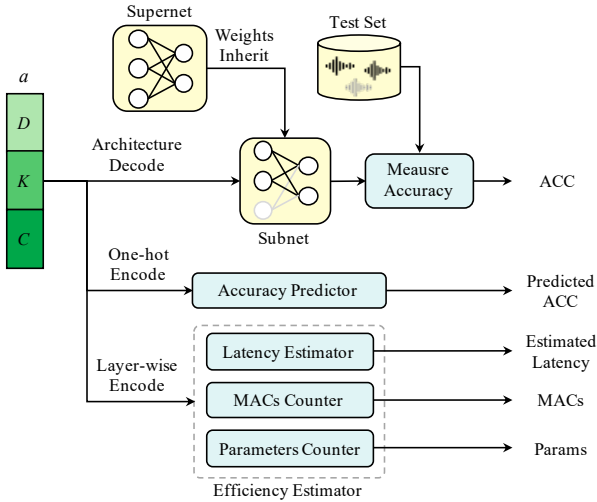


Fig. 6. An overview of subnet evaluation. The accuracy predictor is built based on evaluating sampled architectures from random search. The efficiency estimator consists of latency estimator, MACs counter, and parameters counter. The latency estimator is created by operator-wise measurements, such as evaluating the stem with different widths and kernels. MACs Counter and Parameter Counter are used to calculate MACs and parameters of subnets.

Algorithm 3: Latency-constrained MPEA Fitness

Input: population $\{a_i\}_{i=1}^N$, accuracy predictor f_{ACC} , latency table f_{Lat} , latency threshold Lat_{max}

Output: objective $ObjV$, constraint violation CV

```

1 def Fitness( $\{a_i\}_{i=1}^N, f_{ACC}, f_{Lat}, Lat_{max}$ ):
2    $ObjV \leftarrow \emptyset$ 
3    $CV \leftarrow \emptyset$ 
4   for  $i = 1$  to  $N$  do
5      $x \leftarrow$  encode  $a_i$  as a one-hot vector
6      $ACC \leftarrow f_{ACC}(x)$ 
7      $Lat \leftarrow f_{Lat}(x)$ 
8      $ObjV \leftarrow ObjV \cup ACC$ 
9     if  $Lat \leq Lat_{max}$  then
10       $CV \leftarrow CV \cup 0$ 
11    else
12       $CV \leftarrow CV \cup 1$ 
13    end
14  end
15  return  $ObjV, CV$ 
16 end

```

independent integers. Specifically, the widths of $v_{1 \rightarrow 5}$ are the same, while the widths of $v_{6 \rightarrow 8}$ are three times as large as $v_{1 \rightarrow 5}$, e.g., $(4, \{3\}_{i=1}^5, \{256\}_{i=1}^5 \cup \{768\})$. The coarse-grained space uses sampling space used in the training process, where depth is chosen from $\{2, 3, 4\}$, kernel size is chosen from $\{1, 3, 5\}$, and width is chosen from $\{0.25, 0.35, 0.5, 0.75, 1.0\}$ of the maximum value. Compared to the coarse-grained space, the fine-grained space uses a fine-width of $c = 8$, which provides a subtle solution space.

Under the specific sampling space, the solution to architecture search is to adopt an appropriate search strategy given the solution space, search purpose, and search budget. Exhaustive search is applied if enumerating is available, e.g., for the sampling space of *kernel*. A manually designed grid search is presented based on prior knowledge to analyze the relationship

TABLE III
EXPERIMENTAL SETTINGS OF DATASETS AND TASKS

Task	Dataset	# Utterances / Speakers
Train Supernet	Vox2 Development	1,092,009 / 5,994
Test Supernet	Vox1-O Test	4,708 / 40

TABLE IV
CONSIDERED OPTIONS OF SEARCH SPACE

Dimension	Options	# Options
Depth	2, 3, 4	3
Kernel Size	1, 3, 5	3
Coarse-grained Width $v_{1 \rightarrow 5}$	128, 176, 256, 384, 512	5
Coarse-grained Width $v_{6 \rightarrow 8}$	384, 536, 768, 1152, 1536	5
Fine-grained Width $v_{1 \rightarrow 5}$	128, 136, ..., 512	49
Fine-grained Width $v_{6 \rightarrow 8}$	384, 392, ..., 1536	145

between architecture and accuracy. For a larger solution space, a random strategy is introduced as a baseline to compare to advanced algorithms. Based on random search results, a model predictive evolutionary algorithm (MPEA) is proposed for various objectives, where an efficiency estimator and a surrogate accuracy predictor are established for estimating the efficiency and accuracy of the architecture as [25], [26]. MPEA is an iterative process that in each generation, parents (i.e., promising architectures) and offsprings (i.e., new architectures) compete with each other with a fitness bias for survival and reproduction [40], [41]. The fitness of an individual architecture is a guide to optimize accuracy while constrains latency for selection, as shown in Algorithm 3.

V. EXPERIMENTS EVALUATION

This section presents experimental results to evaluate the effectiveness of EfficientTDNN on VoxCeleb1 and VoxCeleb2 datasets. The details of datasets, supernet, training, search, and evaluation are presented in Section V-A, V-B, V-C, V-D, and V-E. The performance of EfficientTDNN is concluded in Section V-F. Next, generalization to different-grained spaces is presented in Section V-G followed by the trade-off between accuracy and efficiency.

A. Datasets

Experiments are conducted on the VoxCeleb datasets including VoxCeleb1 (Vox1) [16] and VoxCeleb2 (Vox2) [17]. Both corpora are extracted from videos uploaded to YouTube as large-scale speaker recognition datasets collected ‘in the wild’. The statistics of datasets are given in Table III. The VoxCeleb2 development set is used to train the supernet, and the VoxCeleb1-O test set is used to evaluate subnets.

The feature is a 80-dimensional log mel-filterbanks, which is extracted from spectrograms within the given frequency limit 20-7600 Hz. Pre-emphasis is first applied to the input signal using a coefficient of 0.97. Spectrograms are extracted with a hamming window of width 25 ms and step 10 ms with a FFT size of 512. Mean and variance normalization is applied to the feature using instance normalization.

B. Supernet Preparation

Our supernet \mathcal{A} is constructed as Section IV-A. The details of the search space are given in Table IV. According to Theorem 1, the inference time of the subnet $O(a)$ sampled from the supernet is between $O(a_{C2\min})$ and $O(a_{\max})$.

$$a_{C2\min} = (2, \{1\}_{i=1}^3, \{128, 128, 128, 384\})$$

$$a_{\max} = (4, \{5\}_{i=1}^5, \{512, 512, 512, 512, 512, 1536\})$$

Different spaces of the supernet lead to the different lower bound of inference time. For example, for the training task of *kernel*, *depth*, and *width* 1, their minimum inference time are derived from $a_{K\min}$, $a_{D\min}$, and $a_{C1\min}$, respectively,

$$a_{K\min} = (4, \{1\}_{i=1}^5, \{512, 512, 512, 512, 512, 1536\})$$

$$a_{D\min} = (2, \{1\}_{i=1}^3, \{512, 512, 512, 1536\})$$

$$a_{C1\min} = (2, \{1\}_{i=1}^3, \{256, 256, 256, 768\})$$

At the architecture search stage, 10,000 subnets in the coarse-grained space and 10,000 subnets in the fine-grained space are sampled and evaluated on the Vox1-O test set to obtain the pairs of accuracy and architecture. The latency table on Intel Xeon E5-2698 v4 CPU and NVIDIA Tesla V100 GPU are measured in a layer-wise manner using a 3-second utterance to estimate the latency of different architectures.

C. Training Details

The proposed progressive training approach consists of five stages in the sequence of *largest*, *kernel*, *depth*, *width* 1, and *width* 2. Each task added the sampling space as Algorithm 1 is performed under AAM-Softmax [42], [43] loss within 64 epochs using the 16-epoch cyclic learning rate between 10^{-8} and 10^{-3} . The number of dynamic paths M is set to 1 with a uniform sampling strategy for all tasks but *largest*. The *largest* task uses 2-second segments as input with data augmentation that consists of RIR dataset (reverb) [32], MUSAN dataset (music, speech, noise) [44], open-source SoX effects (speedup, slowdown, compand) [45], and SpecAugment (time masking, frequency masking) [33]. The other training tasks use 3-second segments with the data augmentation as the *largest* task except for SpecAugment.

D. Search Details

There are three different approaches, i.e., manual grid search, random search, and MPEA. The manual grid search constrains the search space as $(D, \{K\}_{i=1}^{D+1}, \{C\}_{i=1}^{D+1} \cup \{3C\})$, which contains 441 subnets. The random search considers two different-grained spaces, including the coarse-grained and fine-grained space, and 10,000 subnets in each space are sampled randomly uniformly. In MPEA, a three-layer feedforward neural network with 400 hidden units followed by ReLU in each layer is used as the accuracy predictor. The model is supervised by the mean absolute error between the normalized ground-true and predicted accuracy. MPEA is conducted as a constrained single objective using the Geatpy tool [46] with population 50, mutation 0.1, and generation 200.

TABLE V
COMPARISON OF ACCURACY ON THE VOX1-O TEST BETWEEN EFFICIENTTDNN AND STATE-OF-THE-ART CNN MODELS

Systems	MACs	Params	EER (%)	DCF _{0.01}
D-TDNN ^{*,1} [11]	14.93G	2.36M	1.81%	0.200
ResNet-20 ^{*,2} [6]	12.89G	16.11M	4.30%	0.413
Dual Attention ^{*,2} [49]	4.01G	21.67M	1.60%	-
H/ASP ^{*,2} [48]	3.46G	6.06M	1.18%	-
ARET-25 ¹ [50]	2.9G	12.2M	1.39%	0.199
ECAPA-TDNN ^{*,1} [23]	1.45G	5.79M	1.01%	0.127
Fast ResNet-34 ^{*,2} [30]	672M	1.40M	2.22%	-
AutoSpeech ^{*,3} [27]	3.63G	15.11M	8.95%	-
EfficientTDNN-Mobile	565M	2.43M	1.55%	0.138
EfficientTDNN-SOTA	1.46G	5.85M	0.96%	0.108

E. Evaluation Details

There are two different indexes to evaluated, i.e., accuracy and efficiency. Accuracy reports two metrics, namely, the equal error rate (EER) and the minimum detection cost of the function (DCF_{0.01}). The former is the rate at which both acceptance and rejection errors are equal. The latter is adopted in NIST SRE 2018 [15] and VoxSRC 2019 [47] given $C_{\text{target}} = 0.01$. Their scores are calculated as similar as [48]. Specifically, two 4-second temporal segments are sampled at regular intervals from each test utterance. $2 \times 2 = 4$ cosine similarities are computed from each pair of segments, and their average is used as the score. Before scoring, the mean and standard-deviation of BN1d are calibrated by forwarding batches of inputs since changes of subnets lead to a mismatch of feature maps within layers among different subnets. BN1d is reset using 3-second 6000 utterances in a batch of 32.

Efficiency metrics contain latency, MACs, and parameters. Since the time cost by counting MACs and parameters is non-trivial, a recursive manner that supports dynamic architectural hyperparameters is developed without inference. MACs are measured using a 3-second utterance.

F. Speaker Verification

Pruning a network reduces the requirements of storage and computation but degrades the accuracy. The accuracy of EfficientTDNN is first shown in order to study the effects of the network pruning. Table V reports a comparison between EfficientTDNN and state-of-the-art CNN models on VoxCeleb1 Test, where \star denotes that MACs and parameters are obtained by reproducing the model, and the superscripts of $1/2/3$ represent TDNN-based, ResNet-based, and NAS-based architectures, respectively. EfficientTDNN-Mobile and EfficientTDNN-SOTA are obtained with top-300 adaptive score normalization, in which the imposter cohort consists of the utterance-wise embeddings of 6,000 training utterances.

On the mobile setting ($< 600M$ MACs), EfficientTDNN-Mobile of $(3, \{1, 3, 5, 3\}, \{256, 256, 384, 384, 1152\})$ achieves 1.55% EER and 0.138 DCF_{0.01} with 565M MACs. It outperforms D-TDNN, ResNet-20, Dual-Attention, and Fast ResNet-34 with less storage or computation. It suggests that the search space design borrowed from the ECAPA-TDNN architecture

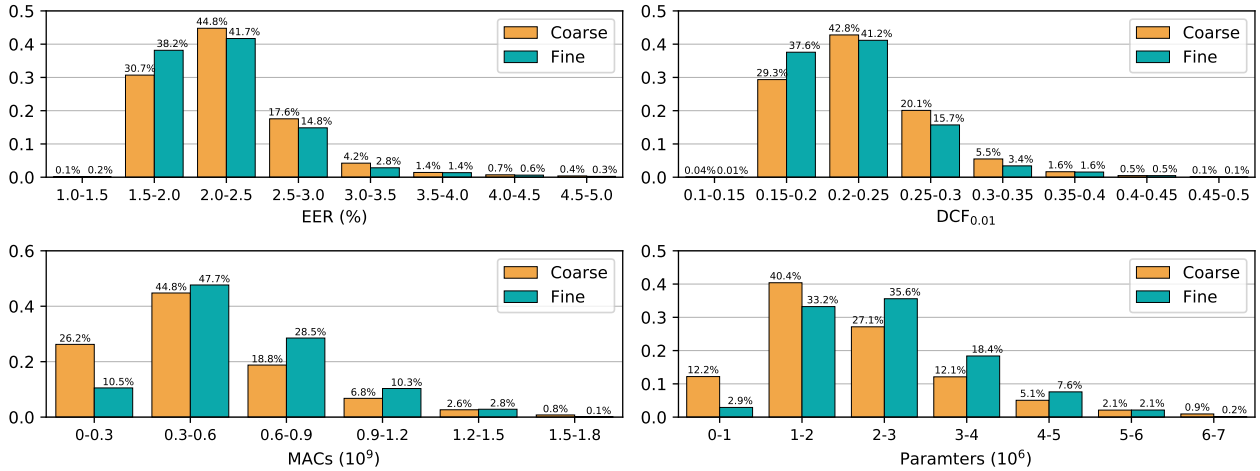


Fig. 7. Distribution of accuracy and efficiency of 20,000 subnets randomly sampled from the coarse-grained and fine-grained spaces. The accuracy includes EER and $DCF_{0.01}$, and the efficiency includes MACs and parameters. The percentage of each bin is given for clarity.

provides a well-behaved supernet, which can create an efficient architecture.

As the budget of storage and computation is neglected, $(3, \{5, 5, 3, 3\}, \{512\}_{i=1}^4 \cup \{1536\})$ derived from the supernet trained after *depth* achieves 0.96% EER and 0.108 $DCF_{0.01}$, as EfficientTDNN-SOTA. The architecture is superior to H/SAP, ARET, and ECAPA-TDNN and achieves state-of-the-art performance. It suggests that the progressive training concerning dynamic kernel and depth can improve the accuracy, which implies the dynamic architecture manner provides an alternative for learning robust speaker embeddings. Also, compared to the NAS solution, AutoSpeech, EfficientTDNN achieves a significant improvement, which is a consequence of designing a search space more suitable for speaker recognition.

G. Generalizing Different-grained Space

Architecture search considers the grain of search space. Two sets of 10,000 subnets are sampled from different-grained spaces randomly, and the distributions of their accuracy and efficiency are illustrated in Figure 7. Since architectures sampled from the fine-grained space do not perform forward during the training process, it is intuitively problematic to achieve favorable accuracy. However, in Figure 7, no subnet from the fine-grained space achieves the accuracy out of the range as that from the coarse-grained space. It implies that the supernet trained progressively generalizes unseen cells.

Furthermore, Figure 7 shows evident differences in EER, $DCF_{0.01}$, MACs, and parameters between the distributions of the coarse-grained and fine-grained space. The accuracy of the subnets sampled from the fine-grained space emphasizes a higher accuracy, e.g., the percentage of the first and second bins is around 38% and 37% compared to around 31% and 29% from the coarse-grained spaces. It probably results from that the subnets sampled from the fine-grained space highlight MACs between 0.3G and 1.2G and parameters between 2M and 5M, as shown in the bottom subfigures of Figure 7. Searching these candidates is helpful to find an efficient architecture capable of computation-limited conditions.

H. Trade-off between Accuracy and Efficiency

As shown in Figure 8, the trade-off between accuracy and efficiency are investigated under different efficiency budgets among multiple metrics and search algorithms, where the accuracy contains EER and $DCF_{0.01}$, the efficiency contains GPU latency, CPU latency, MACs, and parameters, and the algorithm contains random search and MPEA. As the budget of the efficiency increases, the accuracy of the found subnet tends to improve consistently. It indicates that the trained supernet creates such a subnet space that increasing the budget brings accuracy gain.

Remarkably, the predicted accuracy derived from MPEA on the fine-grained space outperforms other methods, as illustrated in Figure 8. However, their actual accuracy has extremely slight improvement and even leads to inferior performance in $DCF_{0.01}$. One reason is that the fine-grained space is significantly larger than the coarse-grained space, which makes it challenging to learn from the number of pairs of accuracy and subnets as equal to the pairs from the coarse-grained. In contrast, the accuracy predictor trained on the coarse-grained space generates approximately equal performance as the actual. It suggests that it is feasible to create an accuracy predictor that learns an appropriate-grained space for finding a subnet with more subtle architectures.

The bottom row in Figure 8 shows that the subnets found by random search achieve superior accuracy, e.g., CPU latency ranges 12ms to 16ms, GPU latency ranges 13ms and 17ms, MACs range 0.8G to 1.0G, and parameters range 1.5M to 4.0M. It suggests that under a specific budget of efficiency, the random search can produce efficient architectures while maintaining $DCF_{0.01}$. It implies that an advanced evolutionary algorithm is not necessary to find an efficient network.

VI. SENSITIVITY ANALYSIS OF ARCHITECTURE SEARCH

In this section, several factors are analyzed by architecture search. First, the performance at different training stages is profiled, and an exhaustive search is applied to illustrate architectures after *kernel* and *depth* training tasks. Next, manual

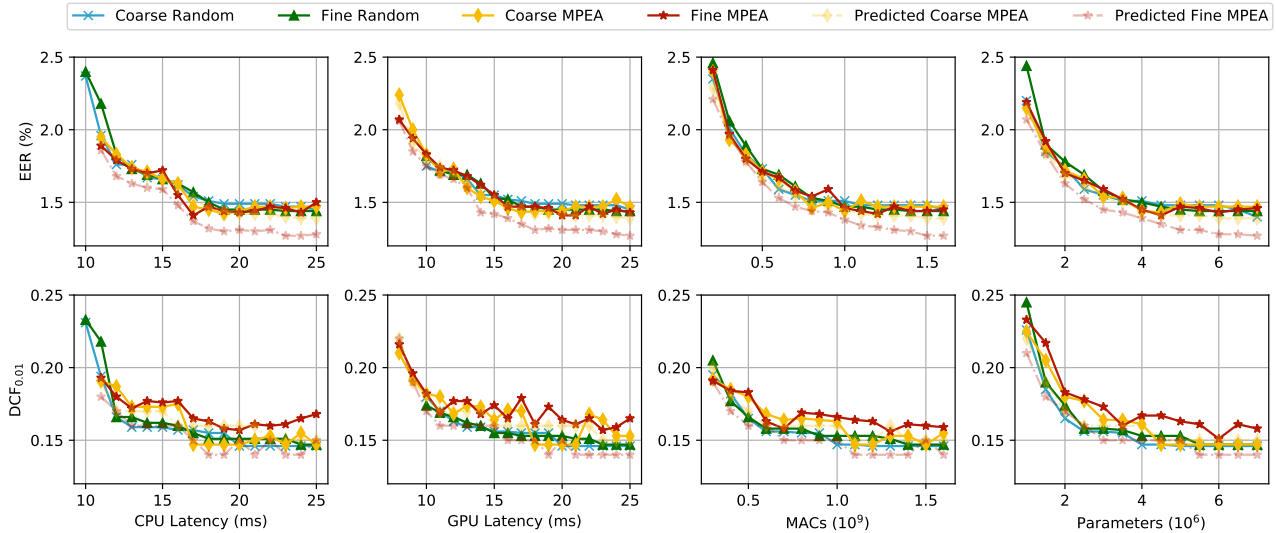


Fig. 8. Trade-off between accuracy and efficiency with different search methods. The top and bottom row depict EER and $DCF_{0.01}$, respectively, as efficiency metrics budget increases. Specifically, the latency is computed by a layer-wise latency estimator using a 3-second utterance. ‘Coarse Random’ denotes random search on a coarse-grained space, and ‘Coarse MPEA’ conducts MPEA on it as the actual accuracy. In contrast, ‘Predicted Coarse MPEA’ reports predicted accuracy from an accuracy predictor. ‘Fine Random,’ ‘Fine MPEA,’ and ‘Predicted Fine MPEA’ are notations similar to ‘Coarse’ methods. In each subfigure, the x-axis denotes the given constraints of an efficiency metric, and the y-axis denotes the accuracy of the found subnet.

TABLE VI
ACCURACY PROFILE AT DIFFERENT TRAINING STAGE ON VOX1-O TEST

Subnet	MACs	Params	<i>largest</i>	<i>kernel</i>	<i>depth</i>	<i>width 1</i>	<i>width 2</i>
			EER(%) / $DCF_{0.01}$	EER(%) / $DCF_{0.01}$	EER(%) / $DCF_{0.01}$	EER(%) / $DCF_{0.01}$	EER(%) / $DCF_{0.01}$
a_{\max}	1.93G	7.55M	1.30% / 0.126	1.18% / 0.122	1.11% / 0.120	1.29% / 0.131	1.44% / 0.163
$a_{K\min}$	1.74G	6.93M	-	3.07% / 0.336	2.79% / 0.308	3.24% / 0.299	3.54% / 0.344
$a_{D\min}$	936.82M	3.98M	-	-	3.18% / 0.315	3.65% / 0.353	3.58% / 0.334
$a_{C1\min}$	267.44M	1.25M	-	-	-	4.12% / 0.405	3.98% / 0.360
$a_{C2\min}$	83.47M	443.97K	-	-	-	-	5.29% / 0.478

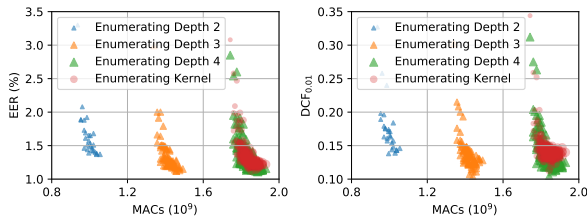


Fig. 9. Distribution between accuracy and efficiency of architectures from enumerating space of *kernel* and *depth*, whose weights are obtained after *kernel* and *depth* training tasks, respectively. The scale of points is the number of parameters.

grid space is used to investigate the relationship between accuracy and depth, kernel, width. Finally, the performance of subnets is reported using different accuracy predictors.

A. Training Stage

Since the supernet creates numerous subnets, it is challenging to determine its performance using a single architecture a_{\max} . To this end, a_{\max} , $a_{K\min}$, $a_{D\min}$, $a_{C1\min}$, and $a_{C2\min}$ are summarized to profile the accuracy of the supernet.

Table VI reports the accuracy of these bounded subnets on the Vox1-O test set. The accuracy varies across different training stages. Specifically, as training tasks undergo from *largest* to *width 2*, the accuracy improves at first but degrades after *width 1*, and a_{\max} derived from the weights of *depth* becomes the optimal solution. It implies that using dynamic kernel and depth during training can benefit the optimization of weights. As Figure 9 shows the distribution between accuracy and efficiency under the weights of *kernel* and *depth*, the weights of *depth* achieve a slight improvement in EER and $DCF_{0.01}$. However, the dynamic width training degrades accuracy. It probably results from that pruning the supernet in width removes such a large number of parameters that causes the problem of over-regularization [51].

Also, the minimal available architecture results in inferior accuracy. For example, the EER of $a_{K\min}$ in *kernel*, $a_{D\min}$ in *depth*, $a_{C1\min}$ in *width 1*, and $a_{C2\min}$ in *width 2* generate lower accuracy. However, architecture accuracy can be improved using the progressive training method. For example, the accuracy of $a_{K\min}$ in *depth* outperforms that in *kernel*, and the $a_{C1\min}$ in *width 2* is superior to that in *width 1*. It suggests that for some specific subnets, training with smaller architectures can achieve accuracy gain. However, $a_{D\min}$ in *width 1* has a lower accuracy than that in *depth*. It probably implies a trade-

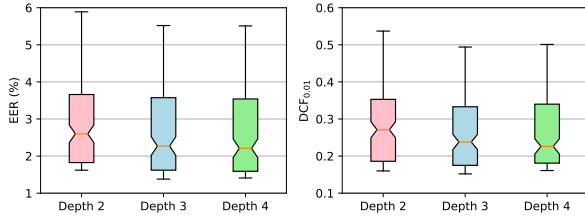


Fig. 10. Distribution between accuracy and depth under grid space, where a box denotes the accuracy of architectures with a specific depth.

TABLE VII
PERFORMANCE OF SUBNETS DERIVED FROM GRID SEARCH AND ANALYSIS ON THE VOX1-O

Subnet	MACs	Params	EER(%)	DCF _{0.01}
$a_{\text{grid}}(3, 3, 384)$	826.11M	3.42M	1.54%	0.148
$a_{\text{grid}}(4, 5, 512)$	1.93G	7.55M	1.44%	0.163

off between pruning smaller subnets while maintaining the accuracy of larger subnets in the supernet training.

B. Architectural Factors

The trained supernet is used to analyze the relationship between accuracy and architectural factors, e.g., network depth, kernel size, and layer width. The grid space is created in the form of $a_{\text{grid}}(D, K, C) \equiv (D, \{K\}_{i=1}^{D+1}, \{C\}_{i=1}^{D+1} \cup \{3C\})$, where D is chosen from $\{2, 3, 4\}$, K is chosen from $\{1, 3, 5\}$, and C is chosen from $\{128, 136, \dots, 512\}$.

1) *Network Depth*: Figure 9 illustrates that depth affects the accuracy of different subnets. In order to investigate the relationship between depth and accuracy, grid space is sampled with different depths. In Figure 10, the architectures with a depth of 2 achieve slightly inferior accuracy compared to that with the depth of 3 or 4, and the accuracy of subnets with depths of 3 and 4 are comparable. It suggests that in the trained supernet, different frame-level features contribute to the accuracy of subnets equally approximately.

2) *Kernel Size*: As shown in Figure 11, the accuracy of the kernel sizes of 3 and 5 significantly outperforms the kernel size of 1 in EER and DCF_{0.01}. It indicates that learning adjacent information helps the model extract discriminative embeddings for speaker recognition. On the other hand, the subnets with a kernel size of 5 have an accuracy similar to that with a kernel size of 3, which means that further increasing the receptive field in the dilated form obtains no accuracy gain. It is safe to conclude that reducing kernel size from 5 to 3 leads to smaller architectures with a slight accuracy loss.

3) *Layer Width*: Figure 12 shows that the increasing width consistently improves the accuracy of subnets. It indicates a monotonic relationship between accuracy and width. Also, the width of around 384 creates an accuracy approximately equal to the largest one. It suggests that reducing the width from 512 to 384 retains the accuracy of subnets but requires less computation and storage.

In summary, the network depth has a slight impact on the accuracy of subnets, while the kernel size and the layer width

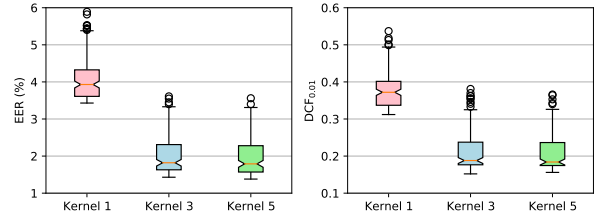


Fig. 11. Distribution between accuracy and kernel size under grid space, where a box denotes the accuracy of architectures with a kernel size.

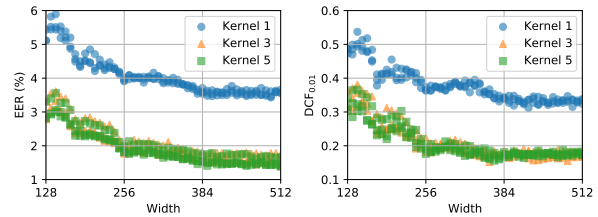


Fig. 12. Distribution between accuracy and width under grid space.

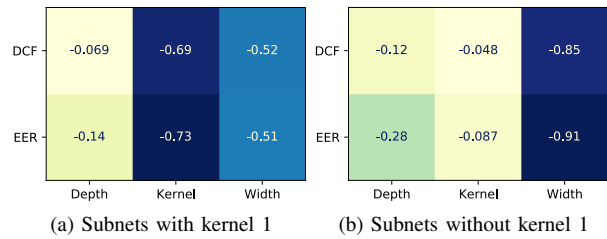


Fig. 13. Spearman rank correlation between accuracy and architectural factors, including network depth, kernel size, and layer width.

are essential and consistent with the spearman rank correlation, as shown in Figure 13a. However, in the absence of subnets with a kernel size of 1, the kernel sizes of 3 and 5 create similarly low correlation coefficients, as illustrated in Figure 13b, which meets the results from the analysis of kernel sizes. We can conclude that the subnet $a_{\text{grid}}(3, 3, 384)$ can achieve a competitive accuracy to the largest one. As shown in Table VII, compared to $a_{\text{grid}}(4, 5, 512)$, the smaller subnet $a_{\text{grid}}(3, 3, 384)$ reduces 57% MACs and 55% parameters while suffers a slight accuracy loss.

C. Accuracy Predictor Performance

Figure 8 indicates that MPEA achieves different accuracy as the predictor varies. The accuracy predictor is conducted with different training data to investigate the relationship between the predicted and actual accuracy. Figure 14 shows performances of selected subnets with 600M MACs among different accuracy predictors. It illustrates that the lower absolute error typically leads to better final results. Furthermore, the coarse-grained space creates subnets superior to the fine-grained space. It suggests that the coarse-grained space predictor is more robust than the fine-grained space predictor. Considering sizes of the fine-grained space are $10^6 \times$ larger sizes of the

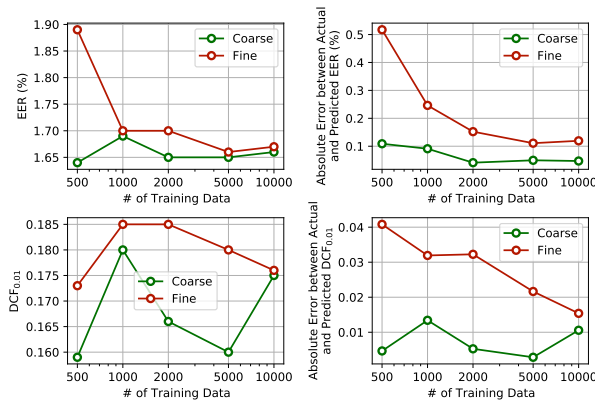


Fig. 14. Performance of MPEA-selected subnets with 600M MACs using predictors with different training data. The right subfigures denote the accuracy, and the left subfigures denote its absolute error between the predicted and actual accuracy.

coarse-grained space, it implies that the increasing number of training data is required for a more subtle space.

VII. CONCLUSION AND FUTURE WORK

In this paper, we address the problem of searching for an efficient network for speaker recognition in the wild that reduces the budget of efficiency while maintains model accuracy. EfficientTDNN is proposed to achieve a trade-off between accuracy and efficiency. Results of experiments on the VoxCeleb dataset show EfficientTDNN enable a significantly large number of architectural settings ($\approx 10^{13}$) concerning depth, width, and kernel sizes. Its resulted architecture at the mobile setting significantly outperforms the NAS alternative, AutoSpeech. It achieves 0.96% EER and 0.108 DCF_{0.01} as the budget of storage and computation is neglected. Furthermore, comprehensive investigation suggests that the trained generalizes cells with more subtle widths and provide an acceptable trade-off between accuracy and efficiency.

However, the limitations of this study are as follows. (1) The designed supernet ranging from 83.47M and 1.93G MACs is not suitable to prune a network since the lower bound of efficiency is so low that large subnets have to adapt to smaller ones, which causes the over-regularization problem. (2) The sensitivity analysis of architectural factors shows that the kernel size of 1 leads to inferior accuracy, but we still consider it as an option for architecture search. (3) The fine-grained space provides subtle architectural hyperparameters options, but it challenges training an accuracy predictor for model predictive search. Therefore, we will make a follow-up future work: (1) Building a supernet that has an appropriately lower bound of network efficiency. (2) Designing an adaptive search method that eliminates options that lead to inferior performance. (3) Establishing a search space that balances the grain of a sampling space and data requirement for training an accuracy predictor.

REFERENCES

[1] J. Villalba, N. Chen, D. Snyder, D. Garcia-Romero, A. McCree, G. Sell, J. Borgstrom, L. P. Garcia-Perera, F. Richardson, R. Dehak, P. A. Torres-Carrasquillo, and N. Dehak, “State-of-the-art speaker recognition with

neural network embeddings in NIST SRE18 and Speakers in the Wild evaluations,” *Comput. Speech Lang.*, vol. 60, p. 101026, 2020.

[2] M. McLaren, L. Ferrer, D. Castan, and A. Lawson, “The speakers in the wild (SITW) speaker recognition database,” in *Proc. INTERSPEECH*, Sep. 2016, pp. 818–822.

[3] S. X. Zhang, Z. Chen, Y. Zhao, J. Li, and Y. Gong, “End-to-end attention based text-dependent speaker verification,” in *Proc. IEEE SLT*, Dec. 2016, pp. 171–178.

[4] S. Yadav and A. Rai, “Learning discriminative features for speaker identification and verification,” in *Proc. INTERSPEECH*, Sep. 2018, pp. 2237–2241.

[5] D. Garcia-Romero, G. Sell, and A. McCree, “MagNetO: X-vector magnitude estimation network plus offset for improved speaker recognition,” in *Proc. ISCA Odyssey*, Nov. 2020, pp. 1–8.

[6] M. Hajibabaei and D. Dai, “Unified hypersphere embedding for speaker recognition,” *arXiv preprint arXiv:1807.08312*, 2018.

[7] D. Snyder, D. Garcia-Romero, and D. Povey, “Time delay deep neural network-based universal background models for speaker recognition,” in *Proc. IEEE ASRU*, Dec. 2015, pp. 92–97.

[8] D. Snyder, D. Garcia-Romero, G. Sell, D. Povey, and S. Khudanpur, “X-Vectors: Robust DNN embeddings for speaker recognition,” in *Proc. IEEE ICASSP*, Apr. 2018, pp. 5329–5333.

[9] D. Povey, G. Cheng, Y. Wang, K. Li, H. Xu, M. Yarmohammadi, and S. Khudanpur, “Semi-orthogonal low-rank matrix factorization for deep neural networks,” in *Proc. INTERSPEECH*, Sep. 2018, pp. 3743–3747.

[10] G. Huang, Z. Liu, L. Van Der Maaten, and K. Q. Weinberger, “Densely connected convolutional networks,” *Proc. IEEE CVPR*, pp. 2261–2269, Jan. 2017.

[11] Y.-Q. Yu and W.-J. Li, “Densely connected time delay neural network for speaker verification,” in *Proc. INTERSPEECH*, Oct. 2020, pp. 921–925.

[12] B. Zoph and Q. V. Le, “Neural architecture search with reinforcement learning,” in *Proc. ICLR*, Apr. 2017.

[13] H. Liu, K. Simonyan, and Y. Yang, “DARTS: Differentiable architecture search,” in *Proc. ICLR*, May 2019.

[14] L. Xie, X. Chen, K. Bi, L. Wei, Y. Xu, Z. Chen, L. Wang, A. Xiao, J. Chang, X. Zhang, and Q. Tian, “Weight-sharing neural architecture search: A battle to shrink the optimization gap,” *arXiv preprint arXiv:2008.01475*, 2020.

[15] S. O. Sadjadi, C. Greenberg, E. Singer, D. Reynolds, L. Mason, and J. Hernandez-Cordero, “The 2018 NIST speaker recognition evaluation,” in *Proc. INTERSPEECH*, Sep. 2019, pp. 1483–1487.

[16] A. Nagrani, J. S. Chung, and A. Zisserman, “VoxCeleb: A large-scale speaker identification dataset,” in *Proc. INTERSPEECH*, Aug. 2017, pp. 2616–2620.

[17] J. S. Chung, A. Nagrani, and A. Zisserman, “VoxCeleb2: Deep speaker recognition,” in *Proc. INTERSPEECH*, Sep. 2018, pp. 1086–1090.

[18] A. Nagrani, J. S. Chung, W. Xie, and A. Zisserman, “Voxceleb: Large-scale speaker verification in the wild,” *Comput. Speech Lang.*, vol. 60, p. 101027, Mar. 2020.

[19] M. McLaren, Y. Lei, and L. Ferrer, “Advances in deep neural network approaches to speaker recognition,” in *Proc. IEEE ICASSP*, Apr. 2015, pp. 4814–4818.

[20] Z. Huang, S. Wang, and Y. Qian, “Joint i-vector with end-to-end system for short duration text-independent speaker verification,” in *Proc. IEEE ICASSP*, Apr. 2018, pp. 4869–4873.

[21] S. Ramoji, A. Mohan, B. Mysore, A. Bhatia, P. Singh, H. Vardhan, and S. Ganapathy, “The leap speaker recognition system for NIST SRE 2018 challenge,” in *Proc. IEEE ICASSP*, May 2019, pp. 5771–5775.

[22] W. Xie, A. Nagrani, J. S. Chung, and A. Zisserman, “Utterance-level aggregation for speaker recognition in the wild,” in *Proc. IEEE ICASSP*, May. 2019, pp. 5791–5795.

[23] B. Desplanques, J. Thienpondt, and K. Demuynck, “ECAPA-TDNN: Emphasized channel attention, propagation and aggregation in TDNN based speaker verification,” in *Proc. INTERSPEECH*, Oct. 2020, pp. 3830–3834.

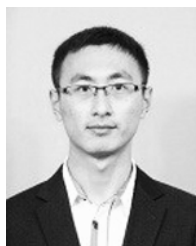
[24] G. Bender, P. J. Kindermans, B. Zoph, V. Vasudevan, and Q. Le, “Understanding and simplifying one-shot architecture search,” in *Proc. ICML*, Jul. 2018, pp. 883–893.

[25] H. Cai, L. Zhu, and S. Han, “ProxylessNas: Direct neural architecture search on target task and hardware,” in *Proc. ICLR*, May 2019.

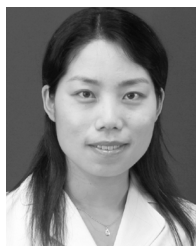
[26] H. Cai, C. Gan, T. Wang, Z. Zhang, and S. Han, “Once-for-all: Train one network and specialize it for efficient deployment,” in *Proc. ICLR*, Apr. 2020.

[27] S. Ding, T. Chen, X. Gong, W. Zha, and Z. Wang, “AutoSpeech: Neural architecture search for speaker recognition,” in *Proc. INTERSPEECH*, Oct. 2020, pp. 916–920.

- [28] X. Qu, J. Wang, and J. Xiao, "Evolutionary algorithm enhanced neural architecture search for text-independent speaker verification," in *Proc. INTERSPEECH*, Oct. 2020, pp. 961–965.
- [29] D. Garcia-Romero, D. Snyder, G. Sell, A. McCree, D. Povey, and S. Khudanpur, "X-vector DNN refinement with full-length recordings for speaker recognition," in *Proc. INTERSPEECH*, Sep. 2019, pp. 1493–1496.
- [30] J. S. Chung, J. Huh, S. Mun, M. Lee, H.-S. Heo, S. Choe, C. Ham, S. Jung, B.-J. Lee, and I. Han, "In defence of metric learning for speaker recognition," in *Proc. INTERSPEECH*, Oct. 2020, pp. 2977–2981.
- [31] T. Ko, V. Peddinti, D. Povey, and S. Khudanpur, "Audio augmentation for speech recognition," in *Proc. INTERSPEECH*, Jan. 2015, pp. 3586–3589.
- [32] T. Ko, V. Peddinti, D. Povey, M. L. Seltzer, and S. Khudanpur, "A study on data augmentation of reverberant speech for robust speech recognition," in *Proc. IEEE ICASSP*, Mar. 2017, pp. 5220–5224.
- [33] D. S. Park, W. Chan, Y. Zhang, C. C. Chiu, B. Zoph, E. D. Cubuk, and Q. V. Le, "SpecAugment: A simple data augmentation method for automatic speech recognition," *Proc. INTERSPEECH*, pp. 2613–2617, Sep. 2019.
- [34] K. Yu, R. Ranftl, and M. Salzmann, "How to train your super-net: An analysis of training heuristics in weight-sharing NAS," *arXiv preprint arXiv: 2003.04276*, 2020.
- [35] K. He, X. Zhang, S. Ren, and J. Sun, "Deep residual learning for image recognition," in *Proc. IEEE CVPR*, Jun. 2016, pp. 770–778.
- [36] J. Hu, L. Shen, S. Albanie, G. Sun, and E. Wu, "Squeeze-and-excitation networks," *IEEE Trans. Pattern Anal. Mach. Intell.*, vol. 42, no. 8, pp. 2011–2023, Aug. 2020.
- [37] S. Gao, M.-M. Cheng, K. Zhao, X.-Y. Zhang, M.-H. Yang, and P. Torr, "Res2Net: A new multi-scale backbone architecture," *IEEE Trans. Pattern Anal. Mach. Intell.*, vol. 43, no. 2, pp. 652–662, Feb. 2021.
- [38] V. Sze, Y.-H. Chen, T.-J. Yang, and J. S. Emer, "Efficient processing of deep neural networks: A tutorial and survey," *Proc. IEEE*, vol. 105, no. 12, pp. 2295–2329, 2017.
- [39] Z. Guo, X. Zhang, H. Mu, W. Heng, Z. Liu, Y. Wei, and J. Sun, "Single path one-shot neural architecture search with uniform sampling," in *Proc. ECCV*, Oct. 2020, pp. 544–560.
- [40] D. Fogel, "An introduction to simulated evolutionary optimization," *IEEE Trans. Neural Netw.*, vol. 5, no. 1, pp. 3–14, 1994.
- [41] Q. Zhang and H. Li, "MOEA/D: A multiobjective evolutionary algorithm based on decomposition," *IEEE Trans. Evol. Comput.*, vol. 11, no. 6, pp. 712–731, 2007.
- [42] J. Deng, J. Guo, N. Xue, and S. Zafeiriou, "ArcFace: Additive angular margin loss for deep face recognition," in *Proc. IEEE/CVF CVPR*, Jun. 2019, pp. 4685–4694.
- [43] X. Xiang, S. Wang, H. Huang, Y. Qian, and K. Yu, "Margin matters: Towards more discriminative deep neural network embeddings for speaker recognition," in *Proc. APSIPA ASC*, no. 2017, Nov. 2019, pp. 1652–1656.
- [44] D. Snyder, G. Chen, and D. Povey, "MUSAN: A music, speech, and noise corpus," *arXiv preprint arXiv:1510.08484*, 2015.
- [45] "Sox - sound exchange," (accessed March 6, 2021). [Online]. Available: <http://sox.sourceforge.net/>, 2015.
- [46] "Geatpy: The genetic and evolutionary algorithm toolbox for python with high performance," (accessed March 6, 2021). [Online]. Available: <http://www.geatpy.com/>, 2020.
- [47] J. S. Chung, A. Nagrani, E. Coto, W. Xie, M. McLaren, D. A. Reynolds, and A. Zisserman, "VoxSRC 2019: The first VoxCeleb speaker recognition challenge," *arXiv preprint arXiv: 1912.02522*, 2019.
- [48] H. S. Heo, B.-J. Lee, J. Huh, and J. S. Chung, "Clova baseline system for the VoxCeleb speaker recognition challenge 2020," *arXiv preprint arXiv: 2009.14153*, 2020.
- [49] J. Li and T. Lee, "Text-independent speaker verification with dual attention network," in *Proc. INTERSPEECH*, Oct. 2020, pp. 956–960.
- [50] R. Zhang, J. Wei, W. Lu, L. Wang, M. Liu, L. Zhang, J. Jin, and J. Xu, "ARET: Aggregated residual extended time-delay neural networks for speaker verification," in *Proc. INTERSPEECH*, Oct. 2020, pp. 946–950.
- [51] H. Xu, D. Luo, R. Henao, S. Shah, and L. Carin, "Learning autoencoders with relational regularization," in *Proc. ICML*, Jul. 2020, pp. 10576–10586.



Rui Wang received the B.S. and M.S. degrees from Zhejiang Sci-Tech University, China, in 2015 and 2018, respectively. He is currently pursuing the Ph.D. degree in computer science and technology from Tongji University, Shanghai, China, under the supervision of Zhihua Wei. His current research interests focus on speaker recognition.



Zhihua Wei received the double Ph.D. degrees in pattern recognition and intelligent system from Tongji University, Shanghai, China, and Lyon University 2, Lyon, France, in 2010. She is currently a Professor at Tongji University. Her current research interests include machine learning, image processing, natural language processing, and speech processing.



Shouling Ji received the Ph.D. degree in electrical and computer engineering from the Georgia Institute of Technology, and the Ph.D. degree in computer science from Georgia State University. He is currently a ZJU 100-Young Professor with the College of Computer Science and Technology, Zhejiang University, and a Research Faculty at the School of Electrical and Computer Engineering, Georgia Institute of Technology. His current research interests include big data security and privacy, big data driven security and privacy, and adversarial learning. He is a member of the ACM. He was the Membership Chair of the IEEE Student Branch at Georgia State (2012–2013).



Zhen Hong received the B.S. degree from Zhejiang University of Technology (China) and University of Tasmania (Australia) in 2006, respectively, and the Ph.D. degree from the Zhejiang University of Technology in Jan. 2012. He was an associate professor with the Faculty of Mechanical Engineering & Automation, Zhejiang Sci-Tech University, China. Since Apr. 2019, he is an associate professor with the Institute of Cyberspace Security, and College of Information Engineering, Zhejiang University of Technology, China. He has visited at the Sensorweb Lab, Department of Computer Science, Georgia State University in 2011. He also has been at CAP Research Group, School of Electrical & Computer Engineering, Georgia Institute of Technology as a research scholar in 2016 to 2018. His research interests include cyber-physical systems, Internet of things, wireless sensor networks, cybersecurity, and data analytics. He received the first Zhejiang Provincial Young Scientists Title in 2013 and the Zhejiang Provincial New Century 151 Talent Project (The Third-Level) in 2014. He also received the 521 Talent Project of Zhejiang Sci-Tech University and the Young and Middle-aged Talents Foundation of Zhejiang Provincial Top Key Academic Discipline of Mechanical Engineering in 2015. He is a member of IEEE, CCF and senior member of CAA, and serves on the Youth Committee of Chinese Association of Automation and Blockchain Committee and CCF YOCSEF, respectively.